

Phase-Contrast X-Ray Imaging Using an X-Ray Interferometer for Biological Imaging

Atsushi MOMOSE,^{†,1} Tohoru TAKEDA,² Akio YONEYAMA,³ Ichiro KOYAMA,¹ and Yuji ITAI²

^{1†} Department of Applied Physics, The University of Tokyo, 7-3-1 Hongo, Bunkyo-ku, Tokyo 113-8656, Japan
(E-mail: momose@exp.t.u-tokyo.ac.jp)

² Institute of Clinical Medicine, University of Tsukuba, Tsukuba, Ibaraki 305-8575, Japan

³ Advanced Research Laboratory, Hitachi, Ltd., Hatoyama, Saitama 350-0395, Japan

The potential of phase-contrast X-ray imaging using an X-ray interferometer is discussed comparing with other phase-contrast X-ray imaging methods, and its principle of contrast generation is presented including the case of phase-contrast X-ray computed tomography. The status of current instrumentation is described and perspectives for practical applications are discussed.

(Received on August 10, 2001; Accepted on October 5, 2001)

Since the discovery of X rays, one has benefited from X-ray imaging using its penetrating property. Nowadays, its application expanded into wide variety of fields such as medicine. The contrast obtained with conventional X-ray imaging is generated by the difference in absorption. Because X-ray absorption coefficient is larger for heavier element, strong contrast is obtained when heavy elements are localizing in an object. On the contrary, when an object mainly consisting of light elements such as biological soft tissue is illuminated with X rays, one encounters a problem that sufficient contrast cannot be generated. Although image quality can be improved by increasing X-ray dose, radiation damage is crucial especially in biological imaging. To overcome this problem, contrast media are occasionally used.

Recently research activity for using phase contrast is growing remarkably in the field of X-ray imaging.¹ This is because one expects that phase-contrast X-ray imaging would give a breakthrough to this problem from a completely different point of view. As mentioned, formation of conventional X-ray transmission images relies on X-ray absorption, and X-ray wave property has not been used for imaging. As illustrated in Fig. 1, when X-ray wave passes an object, its amplitude attenuates by absorption and its phase shifts due to the difference in phase velocity. The advantage of using the X-ray phase shift is that its magnitude is

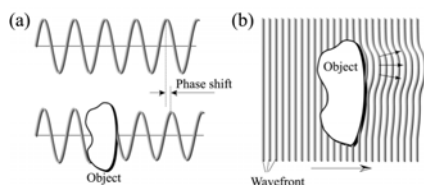


Fig. 1 Illustration describing phase shift. Wavefront is deformed by the phase shift, and this means that propagation direction changes depending on phase gradient as indicated by arrows.

sufficiently large even if absorption is too weak to detect.

This feature can be seen by graphing interaction cross sections of X-ray absorption and X-ray phase shift as a function of atomic number. The absorption cross section corresponds to atomic absorption coefficient μ^a , and the phase-shift cross section can be defined as²

$$p = r_e \lambda (Z + f_1), \quad (1)$$

where r_e , λ , Z , and f_1 are classical electron radius, X-ray wavelength, atomic number, and the real part of anomalous atomic scattering factor. Figure 2 shows μ^a and p for various X-ray energies. In calculation of this, public tables³⁻⁵ for μ^a and f_1 were used. Thus, p is always larger than μ^a , and it should be noted that for light elements the ratio p/μ^a exceeds a thousand. This suggests that extremely high sensitivity would be achieved for biological objects by using X-ray phase information.

From a macroscopic point of view, the phase shift and absorption can be compared by means of complex refractive index $n = 1 - \delta - i\beta$. δ and β are calculated with p and μ^a with

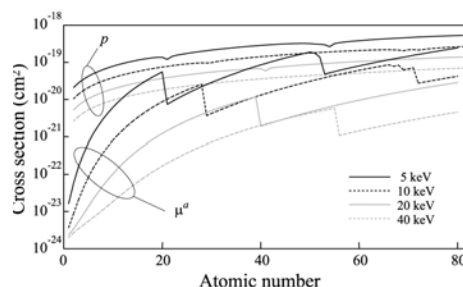


Fig. 2 Interaction cross sections of X-ray absorption (μ^a) and phase shift (p) calculated for various elements. Curves for 5-keV, 10-keV, 20-keV, and 40-keV X rays are shown.

$$\delta = \frac{\lambda}{2\pi} \sum_k N_k p_k \quad (2)$$

and

$$\beta = \frac{\lambda}{4\pi} \sum_k N_k \mu_k^a \quad (3)$$

where N_k is the atomic density of element k . Thus, density and composition affect to δ and β in the same manner, and the difference is attributed to p and μ^a . Therefore, the difference shown in Fig. 2 causes the difference between δ and β almost directly. For instance, the values of δ and β of water are 5.8×10^{-7} and 6.0×10^{-10} for 20-keV X rays. Actually the ratio δ/β is also a thousand.

In this paper, phase-contrast methods studied in the hard X-ray energy region are described, and an example demonstrating its performance expected by the estimation presented above is shown. Finally, perspective of phase contrast X-ray imaging is discussed.

Phase-contrast methods in the X-ray region

Overview

The phase shift cannot be detected by simple measurement of X-ray intensity, and therefore special techniques are required to generate contrast based on the phase shift. Phase-contrast X-ray imaging implies the methods studied for this purpose.

In general, however, choices of optical elements are very limited and furthermore their performances are not always complete in the X-ray region. The performance of conventional X-ray sources is also insufficient for phase-contrast imaging. Therefore, the development of X-ray phase optics was slow until 1980's.

In 1990's, however, research activities of phase-contrast X-ray imaging grew up in connection with the development of 3rd generation synchrotron radiation facilities. In the hard X-ray region, four methods

- Zernike's phase-contrast microscopy⁶
- X-ray interferometry^{2,7,8}
- Diffraction enhancement by a crystal⁹⁻¹¹
- Edge enhancement with a point-like source^{12,13}

are currently studied. The principles of the methods are described briefly below.

Zernike's phase-contrast microscopy

In the visible light region, phase-contrast microscopy developed by Zernike is well known¹⁴ and used widely. Its basic configuration is the same as normal optical microscopy except that an aperture and a corresponding $\lambda/4$ phase plate located at the back focal plane of the objective are added.

In the X-ray region, fabrication of a lens is normally difficult because refractive indices are close to unity, and therefore a Fresnel zone plate is used instead of lens. Recently fine Fresnel zone plates can be fabricated especially for soft X-rays, and phase-contrast soft X-ray microscopy was successfully operated.⁶ Recently, similar trials are also performed in the hard X-ray region.

X-ray interferometry

If an X-ray beam can be divided and combined coherently, X-ray phase information is extracted as interference fringes. In forming X-ray interference optics, however, optical length must be stabilized within the deviation smaller than X-ray wavelength. Therefore, extremely high stability is required for the operation of an X-ray interferometer. Currently, the requirement is met by fabricating an interferometer from a perfect silicon crystal.¹⁵ An X-ray beam can be divided and combined by means of diffraction as shown in Fig. 3. The stability is achieved by cutting the entire body of the interferometer monolithically.

Diffraction enhancement by a crystal

As shown in Fig. 1(b), wavefront is distorted behind an object due to the phase shift. Because the direction of beam propagation is perpendicular to the wavefront, the distortion means that X rays are refracted. Therefore, beam propagation direction varies depending on phase gradient. This method generates contrast by selecting X rays deflected by a certain amount by means of Bragg diffraction at a crystal placed downstream from a sample. Because the angular width of Bragg diffraction is $10^{-5} \sim 10^{-6}$ rad, contrast caused by the refraction is generated owing to the difference in reflectivity at the crystal. Approximately, the contrast is proportional to the phase gradient, although this method is insensitive to the refraction in the direction perpendicular to the scattering plane or the plane spanned by wave vectors of incident and reflected X rays.

Edge enhancement with a point-like source

Another principle is similar to in-line holography. To obtain a hologram, one needs a spatially coherent source or a point-like source. The third-generation synchrotron radiation source partially meets this demand. However, its coherency is still insufficient to carry out ideal holography. Nevertheless, this configuration is attractive because edge enhancement effect appears when the size of a point-like X-ray source is a few tens micron in diameter. Approximately the contrast is proportional to the Laplacian of the phase shift,¹⁶ and therefore contrast depicting structural boundaries is generated.

Advantage of X-ray interferometry

Among the methods described above, we have been studying X-ray interferometry with which one can detect the X-ray phase shift as fringes that correspond to contours of constant phase shift. Generation of fringes means that wavefront is inclined against that of the reference beam, and the spacing of the fringes equals $\lambda/\Delta\theta$, where $\Delta\theta$ is wavefront inclination. Therefore, the smaller the phase gradient is, the easier its detection is. While other methods described above prefer larger beam deflection to generate stronger contrast, it can be pointed out that interferometry is powerful for detecting small beam deflection or small $\Delta\theta$. This property is desirable especially in biological imaging.

Another advantage of X-ray interferometry is easy phase retrieval. An interference pattern is expressed with $\cos \Phi(x, y)$, where $\Phi(x, y)$ is the phase shift and therefore corresponds to a contour map of $\Phi(x, y)$. In general, $\Phi(x, y)$ cannot be determined uniquely from $\cos \Phi(x, y)$, but phase-shifting interferometry¹⁷ enables us to determine $\Phi(x, y)$. In this method, M interference patterns are acquired changing the phase of the reference beam with a step of $2\pi/M$. Then, $\Phi(x, y)$ is calculated with

$$\Phi(x, y) = \arg \left[\sum_{k=1}^M I_k \exp(-2\pi i k / M) \right], \quad (4)$$

where I_k is the interference pattern obtained when the phase of

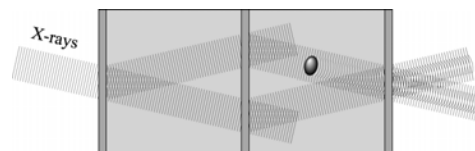


Fig. 3 X-ray interferometer and generated beams. The body of the interferometer is cut out monolithically from an ingot of silicon single crystal. Three wafers work to divide and combine X-ray wave field.

the reference beam is changed by $2\pi k/M$ and $\arg[\]$ implies the extraction of the argument.

This phase retrieval is important because tomographic image reconstruction is realized. $\Phi(x, y)$ is expressed with a projection form of the δ as

$$\Phi(x, y) = \frac{2\pi}{\lambda} \int \delta(x, y, z) dz. \quad (5)$$

This means that a sectional image mapping δ can be reconstructed by measuring the phase map for various projection directions. We have already achieved phase-contrast X-ray computed tomography with this concept,¹⁸ and various biological tissues have been observed so far.¹⁹⁻²²

An example of a phase-contrast tomogram is shown in Fig. 4. The measurement was carried out using synchrotron radiation X rays (17.7 keV) at the Photon Factory, Tsukuba, Japan. Without using contrast media, various structures in human breast tissue are thus revealed.

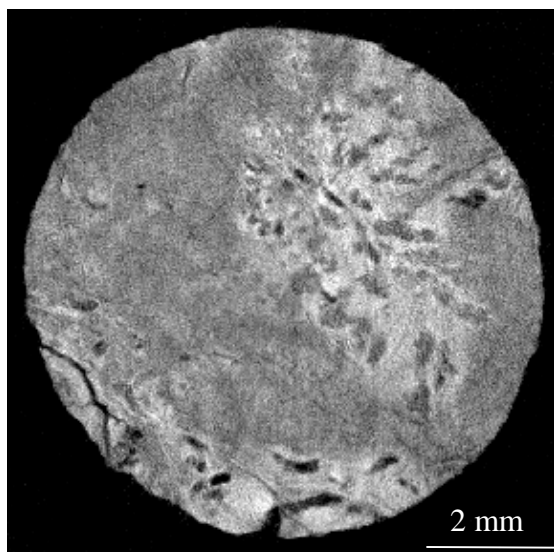


Fig. 4 Phase-contrast tomogram obtained for a tissue piece of human breast.

Perspectives of X-ray interferometric imaging

The δ revealed in a phase-contrast tomogram is approximately proportional to mass density for materials consisting of light elements (see eqs. (1) and (2) and note $f_1 \ll Z$). According to our experimental result obtained for biological soft tissues, it turned out from the signal to noise ratio of phase-contrast tomograms that the sensitivity to density deviation was 7 mg/cm^3 , which corresponded to three times of the standard deviation of the noise.²³

Thus, the sensitivity or contrast resolution of the X-ray interferometric imaging is excellent, and we are conducting a project research to improve this technique in some aspects discussed below aiming at practical applications.

Spatial resolution

The limiting factor of spatial resolution in our phase-contrast imaging is not resolving power of an X-ray image detector nor X-ray source size but the wafer thickness of the X-ray interferometer. According to the geometry shown in Fig. 3, a wafer locates between a sample and an X-ray image detector. As mentioned, the wafer works like an X-ray half mirror. However, owing to the dynamical diffraction of X rays at the wafer, its behavior is extremely sensitive to the angle of incident X rays;

the path of X-ray energy flow inside a crystal is deflected by the amount roughly ten thousand times as large as incident angle deviation. Therefore, X-ray refraction by a sample, which is normally negligible in conventional X-ray imaging, causes image blurring. This effect can be reduced by thinning the wafer, and therefore we are trying to fabricate some X-ray interferometers to improve the spatial resolution.²⁴

Field of view

The field of view depends on the size of the X-ray interferometer, which is limited by the diameter of an ingot of silicon. In order to achieve the stability sufficient for X-ray interference, the X-ray interferometer is cut out monolithically from a floating zone silicon ingot. Therefore, the maximum field of view achieved with this structure is $5 \text{ cm} \times 5 \text{ cm}$ if a 6-inch ingot is used. To generate a field of view larger than this, we need to construct an X-ray interferometer consisting of separated crystal blocks. We are studying the structure shown in Fig. 5, where two crystal blocks with two wafers are used. With this configuration, the maximum field of view can be doubled compared with the monolithic type. Therefore, if a $10 \text{ cm} \times 10 \text{ cm}$ field of view is generated with this configuration, clinical applications such as phase-contrast mammography would become possible. However, the constitution is extremely vibration sensitive, and sub-nanoradian angular control is required to observe interference patterns. Currently, a prototype is successfully operated using synchrotron radiation generating a $2.5 \text{ cm} \times 1.5 \text{ cm}$ field of view by using the technique of phase-lock interferometry. The details of this interferometer are described elsewhere.²⁵

Time resolution

Currently it takes several seconds to observe an interference pattern and about one minute is needed totally to obtain one phase map when synchrotron radiation is used at the Photon Factory. The image acquisition time is determined by X-ray flux available (typically 2×10^6 photons/ mm^2/sec at 17.7 keV). Therefore, time resolution would be achieved by using undulator radiation at 3-rd generation synchrotron radiation facilities, where X-ray brilliance is enough to observe interference patterns with milliseconds time resolution. However, we have to overcome next limiting factor, which is quick phase map acquisition. One possible approach is Fourier transform technique²⁶ introducing fine carrier fringes using for instance a wedge phase shifter instead of using the fringe scanning method. In this case, one phase map can be determined from one interference pattern. However, one has to compromise low spatial resolution because the spatial resolution is larger than carrier fringe spacing in principle.

The fringe scanning method is attractive because of no degrading of spatial resolution. Therefore, we are developing equipment for quick scan of the phase shifter synchronously with the clock of an X-ray image detector. With hardware calculation of phase maps, time resolution below one second would be achieved at 3rd generation synchrotron radiation facilities such as SPring-8, Harima, Japan without degrading spatial resolution.

Other aspects

Phase-contrast X-ray imaging in the other energy region is important and attractive. Our experiments are performed currently around 20 keV. For observation of thick objects, however,

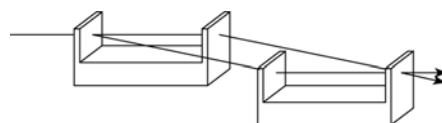


Fig. 5 X-ray interferometer consisting of two independent crystal blocks.

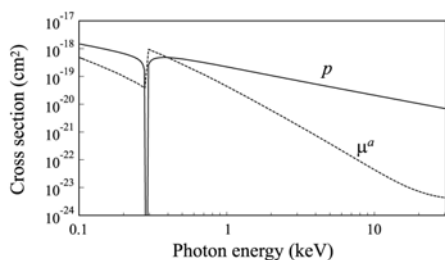


Fig. 6 Interaction cross sections of X-ray absorption (μ_a) and phase shift (p) calculated for carbon as a function of photon energy.

X rays of higher energy should be used. For this purpose, higher quality is required in the fabrication of the X-ray interferometer.

Using soft X-rays are also attractive. Figure 6 shows the cross sections p and μ_a for carbon as a function of X-ray energy. In general, the ratio p/μ_a increases with X-ray energy. This means that phase-contrast methods are powerful when one uses hard X rays. However, at the resonance energy (or absorption edge), p varies tremendously and its value is negative and out of Fig. 6 according to the table⁵ used to calculate Fig. 6. Therefore, if a soft X-ray interferometer is developed, phase-contrast imaging at resonance energies of low-Z elements is attractive. Elementary specific contrast is obtained and furthermore chemical state mapping using XAFS spectra (which is not shown in Fig. 6) would be achieved. No soft X-ray interferometer has been realized so far, and we are trying to achieve the world first using multilayers to divide and combine soft X-ray wave field.

In the hard X-ray region, resonance energies exist for metals, and contrast due to their distribution or chemical state difference would be generated. Using polarization property of synchrotron radiation, phase contrast mapping magnetic state might be obtained. These contrast origins are attractive especially when such elements are distributing to some extent in materials consisting of low-Z elements, because such distributions can be depicted in the existing contrast generated by the normal phase-contrast mechanism.

Conclusions

The status of phase-contrast X-ray imaging using an X-ray interferometer was described including the tomographic method. Although the X-ray interferometer is a delicate device and its handling is not easy, the performance achieved in phase-contrast imaging using it is not realized with other phase-contrast methods. Its applications to biological imaging are therefore attractive despite of the difficulty of instrumentation. The performance has been well demonstrated experimentally so far, and now we are improving some technical aspects aiming at practical applications. If the techniques are established for generating a large field of view and for improving the spatial resolution, new breakthroughs will be brought in biomedical imaging.

Acknowledgements

This study was supported through Special Coordination Funds of the Ministry of Education, Culture, Sports, Science and Technology of the Japanese Government. The experiment using synchrotron radiation was carried out under proposal number 99S2-002 approved by High Energy Accelerator Research Organization.

References

1. R. Fitzgerald, *Phys. Today*, **2000**, 53(7), 23.
2. A. Momose and J. Fukuda, *Med. Phys.*, **1995**, 22, 375.
3. S. Sasaki, "Numerical tables of anomalous scattering factors calculated by the Cromer and Liberman's method" **1989**, KEK Report 88-14, National Laboratory for High Energy Physics, Tsukuba.
4. S. Sasaki, "X-ray absorption coefficients of the elements (Li to Bi, U)" **1990**, KEK Report 90-16, National Laboratory for High Energy Physics, Tsukuba.
5. http://www-cxro.lbl.gov/optical_constants/
6. G. Schmahl, P. Gutmann, G. Schneider, B. Niemann, C. David, T. Wilhein, J. Thieme, and D. Rudolph, in *X-Ray Microscopy IV*, eds. V. V. Aristov and A. I. Erko, Bogorodskii Pechatnik, Chernogolovka, Moscow, **1994**, 196.
7. U. Bonse and M. Hart, *Appl. Phys. Lett.*, **1965**, 7, 99.
8. M. Ando and S. Hosoya, in *Proc. 6th international conference on x-ray optics and microanalysis*, eds. G. Shinoda, K. Kohra, and T. Ichinokawa, Univ. Tokyo Press, Tokyo, **1972**, 63.
9. J. Davis, D. Gao, T. E. Gureyev, A. W. Stevenson, and S. W. Wilkins, *Nature*, **1995**, 373, 595.
10. N. Ingal and E. A. Beliaevskaya, *J. Phys. D*, **1995**, 28, 2314.
11. D. Chapman, W. Thomlinson, R. E. Johnston, D. Washburn, E. Pisano, N. Gmür, Z. Zhong, R. Menk, F. Arfelli, and D. Sayers, *Phys. Med. Bio.*, **1997**, 42, 2015.
12. A. Snigirev, I. Snigireva, V. Kohn, S. Kuznetsov, and I. Schelokov, *Rev. Sci. Instrum.*, **1995**, 66, 5486.
13. S. W. Wilkins, T. E. Gureyev, D. Gao, A. Pogany, and A. W. Stevenson, *Nature*, **1996**, 384, 335.
14. F. Zernike, *Z. Tech. Phys.*, **1935**, 16, 454.
15. U. Bonse and M. Hart, *Appl. Phys. Lett.*, **1965**, 6, 155.
16. A. Pogany, D. Gao, and S. W. Wilkins, *Rev. Sci. Instrum.*, **1997**, 68, 2774.
17. J. H. Bruning, D. R. Herriott, J. E. Gallagher, D. P. Rosenfeld, A. D. White, and D. J. Brangaccio, *Appl. Opt.*, **1974**, 13, 2693.
18. A. Momose, *Nucl. Instrum. Meth. A*, **1995**, 352, 622.
19. A. Momose, T. Takeda, Y. Itai, and K. Hirano, *Nature Medicine*, **1996**, 2, 473.
20. F. Beckmann, U. Bonse, F. Busch, and O. Günnewig, *J. Comput. Assist. Tomogr.*, **1997**, 21, 539.
21. A. Momose, T. Takeda, Y. Itai, A. Yoneyama, and K. Hirano, in *Medical Applications of Synchrotron Radiation*, ed. M. Ando and C. Uyama, Springer-Verlag, Tokyo, 1998, 54.
22. T. Takeda, A. Momose, K. Hirano, S. Haraoka, T. Watanabe, and Y. Itai, *Radiology* **2000**, 214, 298.
23. A. Momose, T. Takeda, Y. Itai, and K. Hirano, in *SPIE Proc. Vol. 2708*, **1996**, 674.
24. K. Hirano and A. Momose, *Jpn. J. Appl. Phys.*, **1999**, 38, L1556.
25. A. Yoneyama, A. Momose, E. Seya, K. Hirano, T. Takeda, and Y. Itai, *Rev. Sci. Instrum.*, **1999**, 70, 4582.
26. M. Takeda, H. Ina, and S. Kobayashi, *J. Opt. Soc. Am.*, **1982**, 72, 156.